

Bayesian regression facilitates quantitative modelling of cell metabolism

Teddy Groves,^{*,†,¶} Nicholas Luke Cowie,^{†,¶} and Lars Keld Nielsen[†]

[†]*The Novo Nordisk Foundation Center for Biosustainability, DTU, Kongens Lyngby, Denmark*

[‡]*Australian Institute for Bioengineering and Nanotechnology (AIBN), The University of Queensland, St Lucia, Australia*

[¶]*These authors contributed equally to this research.*

E-mail: tedgro@biosustain.dtu.dk

Abstract

This paper presents Maud, a command-line application that implements Bayesian statistical inference for kinetic models of biochemical metabolic reaction networks. Maud takes into account quantitative information from omics experiments and background knowledge, as well as structural information about kinetic mechanisms, regulatory interactions and enzyme knockouts. Our paper reviews the existing options in this area, presents a case study illustrating how Maud can be used to analyse a metabolic network and explains the biological, statistical and computational design decisions underpinning Maud.

Keywords

Bayesian inference, kinetic models of cell metabolism, multiomics integration, ordinary differential equations, regulatory analysis

1 Introduction

A kinetic model of cellular metabolism aims to express what is known about a cellular process in the form of an *in silico* representation of the underlying network of chemical reactions. Kinetic models can be used to improve production of target molecules, determine regulatory networks (1) and identify potential drug targets (2, 3). However, the use of kinetic models in practice is hindered by their dependence on noisy and uncertain information sources. Quantitative in vivo measurements of chemical abundances, and in vitro measurements relating to kinetic parameters, both contain vital information but are notoriously inaccurate (4–6). Practically useful kinetic modelling therefore requires a principled statistical approach that encompasses multiple possible model parameterisations.

Bayesian statistical inference can combine the structural information implicit in kinetic models with knowledge about metabolic parameters and information from omics measurements (7, 8). However, kinetic models pose serious computational challenges for Bayesian inference (9, 10).

The scope of a kinetic model is defined by a stoichiometric matrix, S , in which rows represent metabolites, columns represent reactions, and matrix elements s_{ij} represent the stoichiometric coefficient of metabolite i in reaction j . The change in metabolite concentrations is:

$$\frac{dC}{dt} = S \cdot v - \mu \cdot C \tag{1}$$

where C represents a vector of metabolite concentrations, v is a vector of reaction rates, and

μ is the growth rate. The second term represents the dilution due to cell growth.

In a kinetic model, the rates, v , are expressed as a function of the enzyme concentrations, E , the metabolite concentrations, C , and a set of parameters θ :

$$v = f(C, E, \theta) \quad (2)$$

The parameters must include sufficient boundary concentrations and fluxes to solve (1).

It is common to assume pseudo-steady state for metabolites, i.e., the rate of fluxes towards any metabolite is much greater than the rate of change in concentration, $v \gg \frac{dC}{dt}$. Moreover, the dilution effect is assumed minimal, $\mu \cdot C \ll \bar{v}$ (true unless the concentration is very high). Finally, the enzyme concentration is assumed constant for the period considered and hence part of the parameters.

Given these assumptions and a set of values for S , a set of steady state metabolite concentrations and fluxes can be found by solving for C the algebraic equation:

$$S \cdot f(C; \theta) = 0 \quad (3)$$

In a fermentation context, (3) captures the rapid kinetics inside the cell, while another set of ODEs would be used to describe the external substrate and product concentrations, which could act as boundary parameters to (3).

In the context of kinetic modelling, Bayesian inference is appealing because it allows uncertainty to be represented appropriately without sacrificing mechanistic accuracy. Measurement uncertainty can naturally be represented in a Bayesian measurement model, whereas the prior model can represent quantitative uncertainty about kinetic parameters. Finally, kinetic rate laws can be represented in Bayesian data generation models with arbitrarily high fidelity. See Gelman et al. (11) for more details about Bayesian inference and Gelman et al.

(12) for a discussion of practical Bayesian workflow.

Another advantage is that Bayesian inference problems are well-posed even when not all parameters are strongly identified. Sloppy parameter models in which measurable quantities are sensitive to combinations of parameters but not to individual marginal parameter values are ubiquitous in models of biological systems (9, 13). The parameter correlation structure represents the set of potential models that describe the observed data. As we demonstrate later, capturing this correlation structure is difficult outside a fully Bayesian context.

Previous Bayesian kinetic models have either sacrificed mechanistic accuracy or have attempted to fit realistic kinetic models using obsolete or unreliable computational methods.

The most popular algorithm for fitting Bayesian statistical models is Markov Chain Monte Carlo (MCMC). Modern MCMC algorithms enable exploration of high-dimensional posterior distributions, have robust failure diagnostics (14) and can incorporate fast numerical solvers, thereby making inference feasible for Bayesian kinetic models. Nonetheless, the kinetic modelling literature reports an aversion to MCMC, rooted mainly in concerns about sampling time and the presumed difficulty of implementing the required statistical model (7, 15). We are only aware of two recent attempts to implement a Bayesian kinetic modelling approach using MCMC. Stapor et al. (16) fitted detailed kinetic models using relatively inefficient MCMC algorithms that do not scale well to high dimensional parameter spaces limiting the scope of modelling. Conversely, St. John et al. (17) utilises an efficient sampling algorithm but uses approximate kinetics, namely lin-log kinetics (18), limiting the scope of interpreting parameters and inferring cellular behaviour in experimental conditions outside the reference dataset.

There have also been efforts to implement Bayesian inference for kinetic models without the use of MCMC. Examples of alternative inference methods include variational inference (17), rejection sampling and approximate Bayesian computation (7) and Laplace approximation, in which the Fisher information matrix is used to calculate a normal approximation

around the maximum a posteriori parameter configuration (8, 15, 16, 19). Non-MCMC-based Bayesian kinetic models suffer from a lack of reliable diagnostic tools for verifying that their results approximate the target posterior distribution. This is a problem because realistic kinetic models tend to induce highly correlated, non-Gaussian, joint probability distributions (9, 16).

Our application Maud provides a Bayesian kinetic model that combines biologically realistic mechanistic accuracy—including accurate rate laws, post-translational modification and thermodynamics—with fast, robust MCMC sampling using adaptive Hamiltonian Monte Carlo. Further, Maud is a general-purpose application that can be used to fit a wide range of Bayesian kinetic models.

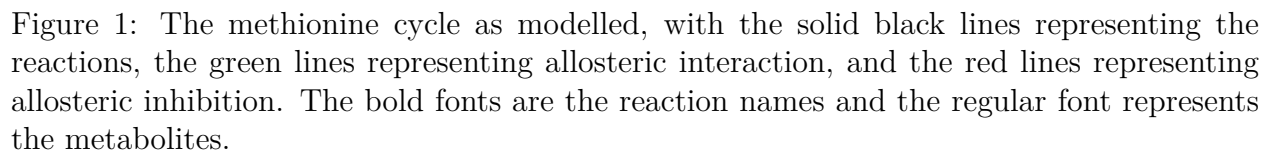
2 Results and Discussion

To demonstrate our application’s capabilities, we used Maud to analyse an artificial dataset based on the human methionine cycle. We generated this dataset using Maud, by simulating measurements for a set of training and validation conditions based on plausible parameter values. Next, we performed posterior inference for the training measurements and prediction for both training and validation measurements.

We investigated Maud’s sensitivity to missing measurements by comparing the results of fitting a full dataset with an intentionally incomplete dataset. To demonstrate why a full Bayesian approach is preferable to an approach based on a Laplace approximation of the posterior distribution, we compared the results of analysing a representative metabolic network using both methods.

Finally, we dug into our results to find out what our full dataset methionine model learned about the contributions of different regulatory factors to the flux through GNMT, an important reaction. This analysis illustrates how Maud can be used to generate actionable insights

The methionine cycle, illustrated in Figure 1, is a fundamental pathway in human metabolism, whose intermediate metabolites participate in a variety of mechanisms which must compete for the same resources. Due to this competition, as well as the fact that all the functions occur simultaneously, the methionine cycle is highly regulated, with 6 known allosteric effectors (20–22). This complex regulation means that quantitative modelling of the methionine cycle requires a detailed kinetic model: this is why we chose it as a case study for Maud.



The simulated dataset and underlying kinetic model that we used for our analysis can be found at https://github.com/biosustain/Methionine_model/tree/main/data/methionine

and is described in supporting information section 3.

We constructed a kinetic model of the methionine cycle in Maud’s format using the description in Korendyaseva et al. (22). The ordinary differential equation system describing this model is

$$\begin{aligned}
\frac{d[met]}{dt} &= v_{Influx} - v_{PROT} - v_{MAT} + v_{MS} + v_{BHMT} \\
\frac{d[amet]}{dt} &= v_{MAT} - v_{GNMT} - v_{METH} \\
\frac{d[ahyc]}{dt} &= v_{GNMT} + v_{METH} - v_{AHC} \\
\frac{d[hyc - L]}{dt} &= v_{AHC} - v_{CBS} - v_{MS} - v_{BHMT} \\
\frac{d[5mthf]}{dt} &= v_{MTHFR} - v_{MS}
\end{aligned} \tag{4}$$

After specifying the qualitative aspects of the kinetic model, we selected parameter values to use as ground truth by Monte Carlo sampling using a previous model of the methionine cycle as a starting point (see Saa and Nielsen (7) for this model).

We used these parameters to simulate steady states in a range of plausible experimental conditions, again using Saa and Nielsen (7) as a starting point. These steady states were then used to generate simulated measurements using the measurement model.

For enzyme and metabolite concentration measurements we specified a standard deviation of 0.1 on natural logarithmic scale, corresponding to approximately 10% measurement error. For each reaction measurement a measurement standard deviation of approximately 10% of the simulated value.

These measurement error specifications are somewhat optimistic considering the many sources of variation and uncertainty affecting quantitative proteomics, metabolomics and fluxomics analyses, but are a reasonable first approximation to a realistic set of

measurements.

For our main model run, we assumed that all metabolite and enzyme concentrations were measured, and that there was a reaction measurement for each of the network’s free fluxes.

The simulated experiments and measurements were split into a training and a validation dataset in a way that achieved a large difference in flux between the two categories. This was done to evaluate whether the fitted model is able to extrapolate to conditions well outside the training dataset rather than merely interpolating between the training data without necessarily learning the system.

We constructed inputs in Maud’s format for each of the analysed datasets, based on the scenario that the true kinetic model was known except for parameter values, which needed to be inferred from the training data and priors. These inputs can be found at https://github.com/biosustain/Methionine_model/tree/main/data.

2.2 Posterior inference

The prior distributions and corresponding true parameter values used in our case study are shown in supporting information section 3.2. They were chosen to reflect a plausible pre-experimental information state. In 7 cases, the marginal prior distribution for a parameter disagrees with the true parameter values used to generate the data; a similar situation is likely to occur in practice due to *in vivo* vs *in vitro* measurement differences.

Running standard diagnostic checks indicated that the samples we generated were from the target posterior distribution. The improved \hat{R} statistic (14) for every variable of interest was within 2% of 1, indicating appropriate mixing within and between Markov chains. Additionally, the number of effective samples was high, indicating that we generated enough posterior samples to support inferences about the bulks of the distributions of the sampled parameters. Furthermore, we observed no post warm-up divergent transitions, indicating that the sampler was able to transform the log-posterior distribution, avoiding any regions

with excessive curvature that might inhibit exploration via HMC.

Posterior predictive checking indicated that our model achieved a good fit to the simulated reaction and metabolite concentration measurements, as shown by the graphs in the top row of Figure 2.

Analysis of the posterior distributions for kinetic parameters indicated that these are highly correlated. The marginal posterior distributions for most kinetic parameters did not shrink significantly compared to the corresponding marginal prior distributions, even though these parameters’ joint posterior distribution contained enough information to make accurate out of sample predictions. In some cases, there were two-dimensional correlations such as the one shown in the bottom left of Figure 2; in this case the marginal distribution of the two parameters is roughly banana shaped. More commonly, however, two-dimensional pair plots were insufficient to reveal the underlying correlation structure, as seen in the bottom-right plot in figure Figure 2, which shows two marginally independent parameters.

These results show that Maud can achieve an adequate fit to a realistic pathway-sized dataset. This was achieved without fixing the marginal values of kinetic parameters: the information required to make good predictions was contained in the correlation structure of the joint posterior distribution. This finding is consistent with previous analyses of biological systems that found they are “sloppy”, that is, sensitive to parameter combinations rather than marginal parameter values, with important combinations, scales and regions of sensitivity being difficult to ascertain in advance (9, 23).

The question naturally arises whether the crucial high-dimensional parameter correlations are linear or non-linear. This is relevant to the question of model performance, as linear correlations are easier to correct for. A linearly correlated posterior space would also be easier to summarise. We address this question in the next section.

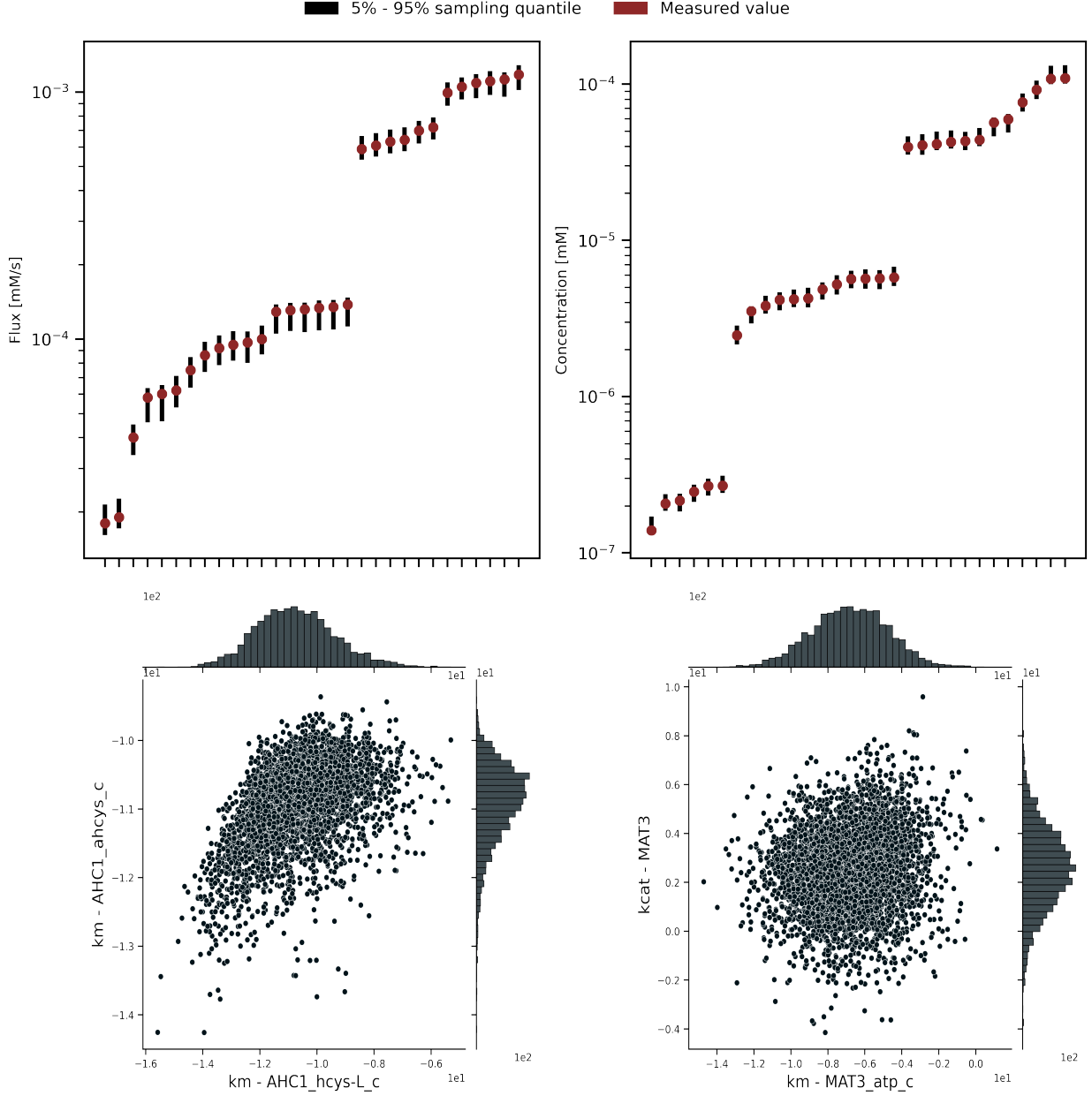


Figure 2: Marginal posterior distributions from our main model run. **(Top left)** Comparison of posterior predictive intervals with simulated flux measurement values. All the flux measurements are within the predictive intervals, indicating a good fit. **(Top right)** Comparison of posterior predictive intervals with simulated concentration measurement values. These also show a good fit. **(Bottom left)** Pairwise marginal posterior distribution for two correlated parameters, namely $K_m^{AHC1,hcys-L}$ and $K_m^{AHC1_ahcys}$. **(Bottom right)** Pairwise marginal posterior distribution for two uncorrelated parameters, namely $K_m^{MAT3,atp}$ and K_{cat}^{MAT3} .

2.2.1 Comparison with Laplace approximation

This current case study illustrates the type of kinetic model and dataset that Maud can fit. The model we analysed has 10 reactions, 5 state variables and 212 parameters. Generalising from our ability to fit this model in a reasonable time using Maud, we expect that Maud can be used to fit realistic Bayesian models of approximately the same size, but not, for example, genome-scale kinetic models. To fit larger models, faster steady state solving methods or alternative inference algorithms will be required. The Laplace approximation, in which the Fisher information matrix is used to calculate a normal approximation around the maximum a posteriori parameter configuration, is a popular strategy for generating approximate posterior samples while avoiding a full MCMC approach.

Using the recently implemented Laplace approximation in Stan, we were unable to generate approximate posterior samples for our main methionine cycle case study using Laplace approximation, as the algorithm could not recover from solver failures caused by unrealistic parameter configurations. This is not an inherent issue of the Laplace transformation but highlights some of the challenges around solving (3) for real problems.

In order still to assess the potential use of the Laplace approximation, we made a comparison for a simpler model. This input can be found at https://github.com/biosustain/Methionine_model/tree/main/data/example_ode. MCMC sampling for this simpler model yielded 800 samples in 625 minutes, while Laplace sampling yielded the same number of samples in only one minute. The diagnostics indicated that our algorithm was able to find the maximum a posteriori parameter configuration, approximate the Hessian and use these quantities to generate approximate posterior samples. The results can be found at https://github.com/biosustain/Methionine_model/tree/main/results.

Comparing the samples generated using each method shows that the Laplace approximation does not provide a good approximation to the true posterior distribution in this case (Figure 3). As can be seen from the top left plot, the total log probability density is clearly

different and this was confirmed by a test of the equality of two empirical univariate distributions (Kolmogorov-Smirnov, $p = 1.7 \times 10^{-65}$).

The difference between the Laplace approximation output and the true posterior distribution manifests not only in the parameter space, but also in the measurement space for both training data (upper right) and validation data (lower left). The lower log likelihood values indicate that the modelled and measured values are further away and that the Laplace approximation yielded significantly worse predictions than the true posterior, even for the training data.

To further explore why this is the case we compared samples from the true posterior and the Laplace approximation for the pairwise marginal distributions of two Michaelis-Menten constants $K_m^{A,r1}$ and K_{cat}^{r1} (Figure 3, bottom right). This comparison demonstrates that the Laplace method is not able to capture the correct relationships between parameters' distributions.

This result shows that MCMC, while slower than Laplace approximation, is required for posterior inference in this case. We expect that the Laplace method will produce worse approximations the more complex the target model. Since the approximation is already unacceptable for our simple test model, we recommend that Maud users use MCMC sampling in preference to Laplace approximation if possible when fitting realistic Bayesian kinetic models.

Our results here also provide circumstantial evidence that the parameter correlations in Bayesian kinetic model posteriors tend to be non-linear, as a posterior with only linear correlations would likely be more germane to Laplace approximation. A conclusion that we drew from this analysis was that the results of fitting our model cannot be summarised simply, for example by fitting a multivariate normal distribution to the posterior draws. We therefore recommend that Maud users store the full set of MCMC draws rather than using such an approximation. This does not preclude the possibility that there is an alternative,

more compact, way to summarise the results of Bayesian kinetic model inference; we leave research into this topic to future work.

2.3 Effect of missing metabolite concentration measurements

To gain insight into our model’s robustness to missing measurements, we also performed a model run with the same 6 experimental datasets, but with measurements of the metabolite S-Adenosyl-L-homocysteine, or “ahcys” removed. Since ahcys regulates three enzymes in the methionine cycle, including one enzyme which is also thermodynamically regulated, we expected the removal of these measurements to yield interesting results.

Comparing model runs with and without the ahcys measurements showed that Maud can produce sensible results even from incomplete metabolomics data.

As might be expected, the model with missing measurements did not correctly infer the missing ahcys concentrations (Figure 4). Nonetheless, the remaining measured metabolites were still well predicted, suggesting that information about the network is still preserved despite the missing measurements. Comparison of flux measurements in both models also indicated that removing the ahcys measurement did not result in catastrophic model failure.

The missing measurements did affect Maud’s ability to infer parameter values correctly (Figure 4, lower left). The model with full metabolomics learned the true value for the displayed dissociation constant, despite this value being far from the mean of the corresponding marginal prior distribution. In contrast, the model with missing measurements stayed in the neighbourhood of the prior.

This result is reassuring because not having access to all measurements is a common situation in multi-omics studies. For instance, measuring all metabolites in a pathway can be infeasible because of limitations of mass spectrometers, availability of standards, column effects, and compartmentalisation. However, provided that sufficient information is available from other sources, our approach can produce sensible results from incomplete metabolomics data.

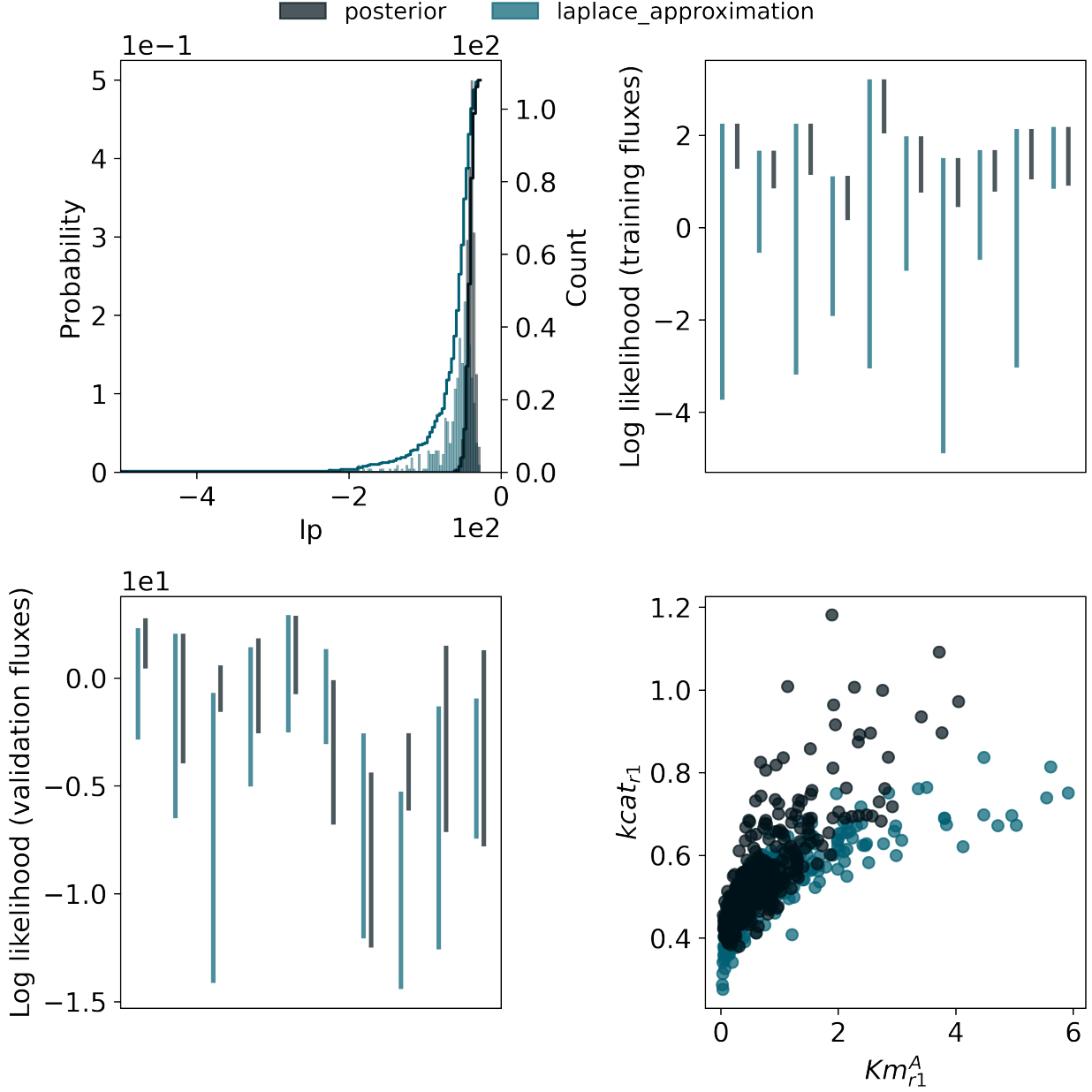


Figure 3: Graphical comparison of approximate posterior samples generated using Laplace sampling (blue-green) with posterior samples generated using MCMC (dark grey). (**Top left**) the two sets of samples clearly have different marginal distributions for the overall log probability variable, indicating that the Laplace samples do not accurately approximate the target distribution. (**Top right**) The distribution of marginal posterior predictive log likelihood values for training data flux measurements shows that the Laplace method tended to yield much worse predictions compared with the true model (lower log likelihood values indicate that the modelled and measured values are further away). (**Bottom left**) The Laplace method also tended to produce worse flux predictions for held-back test measurements. (**Bottom right**) The marginal joint distribution of two parameters: $K_m^{A,rl}$ and K_{cat}^{r1} . The Laplace method is not able to track the correct joint distribution for this pair of parameters. This is unsurprising given that the target distribution has position-dependent scales which are difficult for a linear approximation to capture.

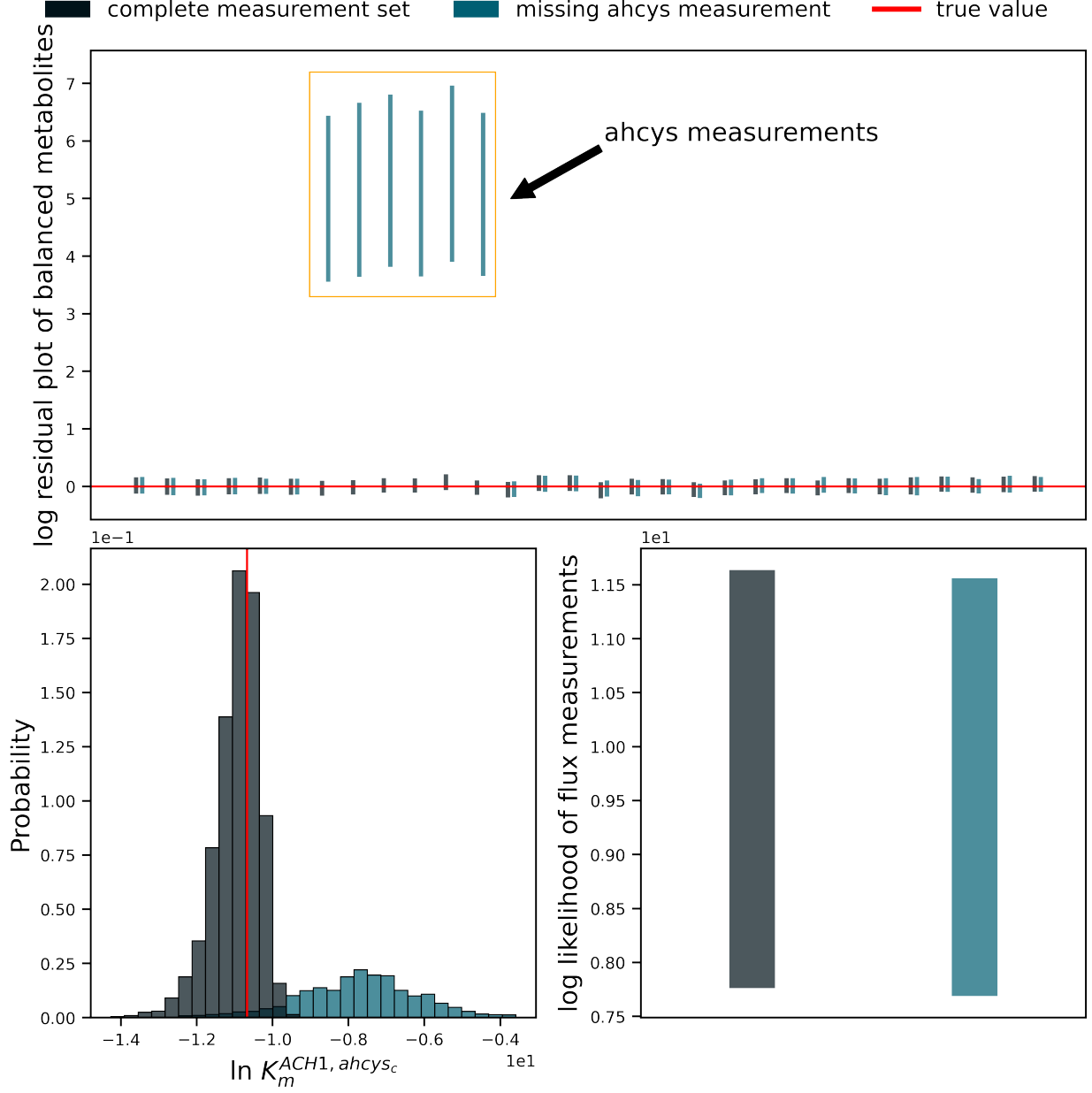


Figure 4: Results of removing concentration measurements for the metabolite $ahcys_c$ from our case study dataset. **(Top)** A comparison of metabolite concentration residuals between the full measurement dataset (blue-green) and the missing-data dataset (grey), displayed on natural logarithmic scale. The missing-data model was unable to estimate the withheld $ahcys_c$ concentrations. **(Bottom Left)** The marginal posterior distribution for the Michaelis constant $K_m^{ACH1, ahcys_c}$ in each model, alongside the true parameter value used to generate both datasets. The true value is recovered by the complete-data model but not by the missing-data model. **(Bottom Right)** The distribution of total log-likelihood for out-of-sample flux measurements in both models. There is a significant overlap between the two distributions, suggesting that removing the $ahcys_c$ measurement did not cause catastrophic prediction failure. However, overall the complete-data model tended to make better predictions.

2.4 Application to regulatory understanding

To demonstrate how Maud’s output can be used to yield useful metabolic insights we used the results of our case study to explain why the flux of the enzyme GNMT is higher in dataset 1 than in dataset 12 (Figure 5). GNMT is an irreversible enzyme that is homotropically activated by its substrate, competitively inhibited by its product and heterotropically inhibited by 5,10- methylenetetrahydrofolate (mlthf). The complex regulation makes it the ideal test case to elucidate regulatory changes.

Regulation can be separated into enzyme abundance, allostery and saturation, and we can plot the marginal posterior distribution of the ratio of the corresponding regulatory component in dataset 1 compared with dataset 12 (Figure 5, right panel). A positive value indicates that the component was increased in dataset 1 relative to dataset 12, with 0 indicating no difference. The probability, according to our model, of the component acting in each direction is given by the relative area under the curve on each side of the zero point.

Our model correctly inferred that saturation and allosteric effects were the main drivers of regulation between the two datasets in this case, with the curves for each component aligning with the ground truth shown in red.

Importantly, this form of analysis takes into account all modelled sources of uncertainty, including uncertainty about the measured values of the flux in each dataset. Our result shows that Maud could be used in this realistic case not only to explain an observed difference in fluxes, but also to provide a reasonable judgement as to the explanation’s robustness.

3 Methods

Maud is a command line application implementing Bayesian inference for a wide range of realistic kinetic models. Maud is written in Python (24), designed for use on Windows, macOS and Linux, is `pip` installable from the Python Package Index as `maud-metabolic-models`,

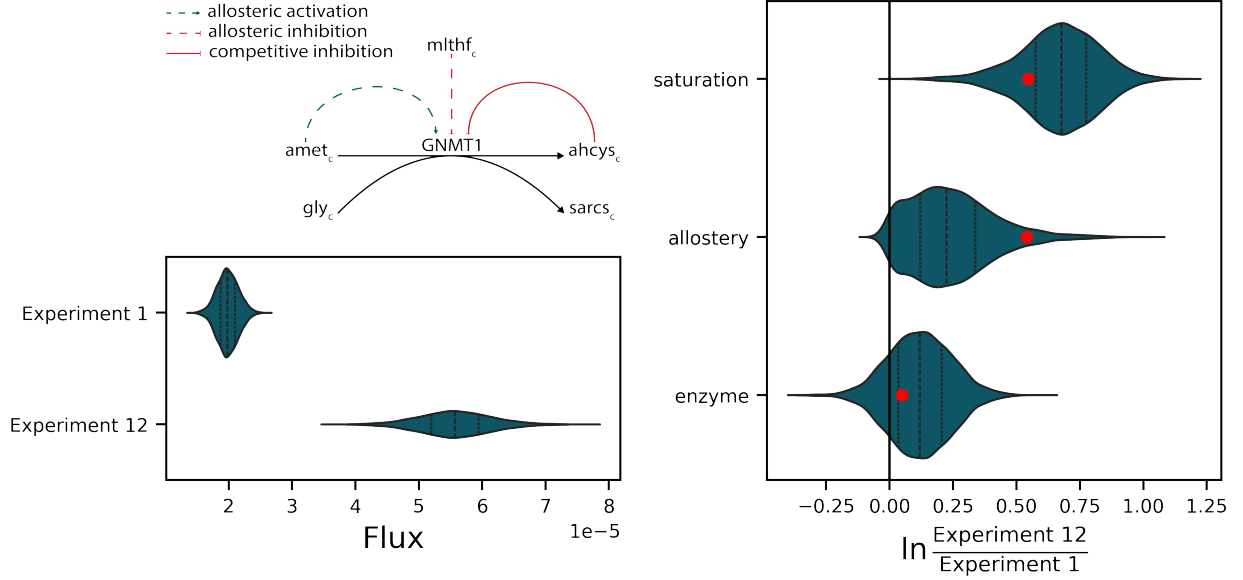


Figure 5: Illustration of how analysing a system with Maud can yield actionable insights about the underlying metabolic network. **(Top Left)** A schematic of the regulatory interactions associated with the enzyme *GNMT1*. Dashed green lines represents allosteric activation, dashed red lines indicate allosteric inhibition and solid red lines represent competitive inhibition. **(Bottom Left)** Comparison of marginal posterior distributions for *GNMT* flux in datasets 1 and 2. **(Right)** Log-scale ratios of the regulatory elements defined in (5). Note that the *Reversibility* and k_{cat} components are excluded: this is because this reaction was modelled as irreversible, and k_{cat} was modelled as constant across datasets. These plots identify why flux in dataset 12 is higher than in dataset 1: the flux increase is due to allostery and saturation with no control from enzyme concentration changes.

documented at <https://maud-metabolic-models.readthedocs.io> and actively developed and maintained at <https://github.com/biosustain/Maud/>.

To use Maud, a user must first collate appropriate input information, represent it in files with Maud’s required formats (see supporting information section on input format). Maud’s command line interface provides commands for inference via a range of algorithms including adaptive Hamiltonian Monte Carlo, as well as commands for simulation and making out-of-sample predictions. Results are stored in files, using a structured, interoperable format.

As well as parameter values, Maud also performs inference for derived quantities including the components of the regulatory decomposition described below in (5), log likelihoods, simulated measurement values and metabolic control analysis coefficients (25).

In the rest of this section we describe Maud’s kinetic model at high level and discuss Maud’s statistical model, implementation and how it solves the crucial steady state problem. Further details about Maud’s kinetic model can be found in the supporting information.

3.1 Kinetic model

Maud’s kinetic model decomposes into factors:

$$F(C; \theta) = \textit{Enzyme} \cdot k_{cat} \cdot \textit{Reversibility} \cdot \textit{Saturation} \cdot \textit{Allostery} \quad (5)$$

Each of the terms on the right-hand side of (5) is a function of C and θ . This idea is taken from Noor et al. (26). The terms usefully gather physically meaningful and conceptually distinct factors contributing to reaction fluxes. *Enzyme* captures the effect of enzyme concentration, k_{cat} that of enzyme efficiency, *Reversibility* quantifies thermodynamic effects, *Saturation* the effect of enzyme availability and *Allostery* the effect of post translational modifications.

We used the model of enzyme saturation from Liebermeister et al. (27) and the generalised

Monod-Wyman-Changeux model of Allosteric regulation introduced in (28–31) and used more recently in Matos et al. (32). To capture the effect on enzyme activity of coupled phosphorylation and dephosphorylation processes we developed a new mathematical model inspired by the generalised MWC model of allosteric regulation. Full details of all mathematical aspects of Maud’s kinetic model can be found in supporting information section 2.

3.2 Statistical model

Maud represents information from measurements using generalised linear regression models that probabilistically connect realised measurements with true values of the measurable quantities. Information from other sources is represented using a prior distribution over a set of latent parameters. The parameters and the measurable quantities are connected by a generative model encompassing Maud’s kinetic model as well as the steady state equation (3). Together, the measurement model, prior model and generative model determine a joint probability function that assigns a probability density to any possible combination of measurements and parameters.

Below we describe the prior and measurement models, as the generative model has already been discussed above.

3.2.1 Prior model

Maud’s prior model includes unknown parameters corresponding to quantities in the kinetic model that are assumed to be unknown, other than steady state metabolite concentrations and fluxes, which are derived from the values of other parameters by solving the steady state problem. See table 1 in this paper’s supporting information for a description of all these parameters and their dimensions.

Except for metabolites’ standard condition Gibbs energy changes of formation, Maud uses

independent normal prior distributions for parameters that can in principle be both negative and positive. For parameters that are constrained to be positive, Maud uses independent log-normal distributions. Formation energy parameters have a multivariate normal prior distribution. Location, scale and covariance parameters for all these prior distributions can be selected freely by the user.

3.2.2 Measurement model

Maud’s measurement model considers three types of measurement: metabolite concentration measurements, enzyme concentration measurements and flux measurements, represented by vectors y^{conc} , y^{enz} and y^{flux} respectively.

All measurements are specific to an experimental condition; that is, a case where the true state of the network, including knockouts, boundary conditions and state variables as well as kinetic and thermodynamic parameters, can safely be assumed to be the same. Maud’s statistical model allows for arbitrarily many experimental conditions, and for any measurable quantity to be measured any number of times in any condition.

Metabolite and enzyme measurements are intended to represent the results of quantitative metabolomics and proteomics experiments. The likelihood functions for such measurements are:

$$y_i^{conc} \sim LN(\ln \hat{y}_i^{conc}, \sigma_i^{conc}) \quad (6)$$

$$y_i^{enz} \sim LN(\ln \hat{y}_i^{enz}, \sigma_i^{enz}) \quad (7)$$

Both equations are log-normal generalised linear models with a standard link function (the natural logarithm \ln) and known standard deviation σ . The use of this measurement model is motivated by the consideration that concentrations are constrained to be non-

negative, so the measurement model should avoid assigning positive probability mass to negative metabolite concentration values. In addition, we expect the precision of most metabolomics and proteomics experiments to be roughly proportional to the true value of the measured quantity, which supports a measurement model with constant coefficient of variation. The measurement standard deviations σ_{conc} and σ_{enz} are assumed to be known exactly for simplicity; plausible values can be elicited by considering the likely coefficient of variation of the measuring apparatus. Our measurement model improves on analyses of metabolomics and proteomics data that assume a regression model with normally distributed errors, whether explicitly using a standard linear model or implicitly using ordinary least squares fitting.

Flux measurements, representing the results of quantitative fluxomics analyses, are modelled using a likelihood function from a standard linear regression model (8). Flux measurements can be obtained from isotope labelling experiments using metabolic flux analysis, for example as described in (Young 2014). When entering flux measurements, it is important only to specify measurements for a network’s free fluxes, as the values of some steady state fluxes in a metabolic network are constrained by others, with the result that dependent fluxes cannot typically be measured separately. If measurements of multiple dependent fluxes are entered, information will inappropriately be double counted.

$$y_i^{flux} \sim LN(\ln \hat{y}_i^{flux}, \sigma_i^{flux}) \tag{8}$$

The use of independent measurement models for metabolite, enzyme and flux measurements carries an implicit assumption that there are no systematic correlations in the measurement errors. This choice was motivated by simplicity - it would be better to use a model with potentially correlated measurements. Similarly, it would be preferable to include measurement errors as model parameters, thereby avoiding possible bias due to incorrect assessments of measurement accuracy. However, we chose to use a simpler measurement model to avoid

the complexity and potential fitting issues that these changes would entail.

Finally, the reader may wonder why Maud uses a linear regression model for reaction flux measurements even though this creates the potential for erroneous double counting and requires non-trivial upstream modelling, as intracellular fluxes typically cannot be measured directly. Instead, fluxes are typically inferred from isotope labelling experiments using metabolic flux analysis: see Dai and Locasale (33) for more about this method. Ideally Maud’s measurement model for fluxes would extend from fluxes to the results of potential labelling experiments, thereby removing the need for upstream analysis and avoiding any double counting. This option has not yet been pursued, again for the sake of simplicity.

3.3 Implementation

Maud uses the Python library `click` (34) to implement a command line interface. The command line interface loads input files as Python dictionaries, which are parsed using the Python library `toml` (35) and then validated and converted into structured `MaudInput` objects using `Pydantic` (36). Maud’s statistical model is implemented in the probabilistic programming language `Stan` (37) and accessed using the interface `cmdstanpy` (38). For posterior sampling, Maud uses the `MaudInput` to create an input file for `Stan` and then trigger posterior sampling using adaptive Hamiltonian Monte Carlo. See Betancourt (39) for more about this algorithm.

When sampling is complete, Maud converts the output into the standard format `InferenceData` using the Python library `arviz` (40) and saves it as a json file, along with some information for debugging. This format allows for easy checking of MCMC diagnostics including divergent transitions, effective sample size and the improved \hat{R} statistic proposed in Vehtari et al. (14).

3.4 Solving the steady state problem

Maud’s parameters are connected with measurable quantities via the steady state equation (3). Posterior sampling using adaptive Hamiltonian Monte Carlo requires repeatedly solving (3) and finding the gradients of its solution with respect to all model parameters. This must be done numerically as analytic solutions are not available for realistic kinetic models.

The speed at which this problem can be solved is tightly coupled with the size and complexity of metabolic network that can practically be modelled. See Timonen et al. (41) for more about considerations involved in this kind of modelling.

To solve (3) and find its gradients, Maud uses a hybrid method involving two numerical solvers from the SUNDIALS suite (42): CVODES and IDAS via their interface from Stan. The hybrid method follows that proposed by Margossian (43), and involves numerically evolving the ODE system for a short period of time, then using the difference between the evolved and starting concentrations as the target for a numerical algebra solver.

4 Supporting information

The analyses described in this paper, as well as instructions for reproducing our results, figures and paper, can be found at https://biosustain/Methionine_model.

The document `supporting_information.pdf` contains the following information:

- Description of Maud’s input format.
- Description of Maud’s kinetic model including rate equations as well as parameters and their dimensions.
- Details of the procedure used to generate our case study results, including generating the artificial case study datasets, specifying priors and carrying out computation.
- Specification of the prior distribution used for the case studies.

5 Acknowledgements

This research was funded by the Novo Nordisk Foundation (Grant numbers NNF20CC0035580 NNF14OC0009473).

6 References

1. Christodoulou, D., Link, H., Fuhrer, T., Kochanowski, K., Gerosa, L., and Sauer, U. (2018) Reserve Flux Capacity in the Pentose Phosphate Pathway Enables *Escherichia coli*’s Rapid Response to Oxidative Stress. *Cell Systems* 6, 569–578.e7.
2. DeBerardinis, R. J., and Chandel, N. S. (2016) Fundamentals of cancer metabolism. *Science Advances* 2, e1600200.
3. Liberti, M. V. et al. (2017) A Predictive Model for Selective Targeting of the Warburg Effect through GAPDH Inhibition with a Natural Product. *Cell Metabolism* 26, 648–659.e8, [tex.pmid: 28918937](#) [tex.publisher: Cell Press](#).
4. Siskos, A. P., Jain, P., Römisch-Margl, W., Bennett, M., Achaintre, D., Asad, Y., Marney, L., Richardson, L., Koulman, A., Griffin, J. L., Raynaud, F., Scalbert, A., Adamski, J., Prehn, C., and Keun, H. C. Interlaboratory Reproducibility of a Targeted Metabolomics Platform for Analysis of Human Serum and Plasma. 89, 656–665.
5. Tabb, D. L. et al. Repeatability and Reproducibility in Proteomic Identifications by Liquid Chromatography–Tandem Mass Spectrometry. 9, 761–776.
6. Lu, W., Su, X., Klein, M. S., Lewis, I. A., Fiehn, O., and Rabinowitz, J. D. Metabolite Measurement: Pitfalls to Avoid and Practices to Follow. 86, 277–304.
7. Saa, P. A., and Nielsen, L. K. (2016) Construction of feasible and accurate kinetic models of metabolism: A Bayesian approach. *Scientific Reports* 6, 29635.

8. Gopalakrishnan, S., Dash, S., and Maranas, C. (2020) K-FIT: An accelerated kinetic parameterization algorithm using steady-state fluxomic data. *Metabolic Engineering*
9. Gutenkunst, R. N., Waterfall, J. J., Casey, F. P., Brown, K. S., Myers, C. R., and Sethna, J. P. (2007) Universally sloppy parameter sensitivities in systems biology models. *PLoS Computational Biology* *3*, 1871–1878, [tex.pmcid: PMC2000971](#) [tex.sciwheel-projects: Relative Metabolomics](#).
10. Raue, A., Becker, V., Klingmüller, U., and Timmer, J. (2010) Identifiability and observability analysis for experimental design in nonlinear dynamical models. *Chaos: An Interdisciplinary Journal of Nonlinear Science* *20*, 045105.
11. Gelman, A., Carlin, J. B., Stern, H. S., Dunson, D. B., Vehtari, A., and Rubin, D. B. (2020) Bayesian Data Analysis, Third Edition. 656.
12. Gelman, A., Vehtari, A., Simpson, D., Margossian, C. C., Carpenter, B., Yao, Y., Kennedy, L., Gabry, J., Bürkner, P.-C., and Modrák, M. (2020) Bayesian Workflow. *arXiv:2011.01808 [stat]*
13. White, A., Tolman, M., Thames, H. D., Withers, H. R., Mason, K. A., and Transtrum, M. K. (2016) The limitations of model-based experimental design and parameter estimation in sloppy systems. *PLoS Computational Biology* *12*, e1005227, [tex.pmcid: PMC5140062](#) [tex.sciwheel-projects: Relative Metabolomics](#).
14. Vehtari, A., Gelman, A., Simpson, D., Carpenter, B., and Bürkner, P.-C. (2021) Rank-Normalization, Folding, and Localization: An Improved \hat{R} for Assessing Convergence of MCMC (with Discussion). *Bayesian Analysis* *16*, 667–718.
15. Raue, A., Kreutz, C., Theis, F. J., and Timmer, J. (2013) Joining forces of Bayesian and frequentist methodology: a study for inference in the presence of non-identifiability. *Philosophical Transactions of the Royal Society A: Mathematical, Physical and Engineering Sciences* *371*, 20110544.

16. Stapor, P., Weindl, D., Ballnus, B., Hug, S., Loos, C., Fiedler, A., Krause, S., Hroß, S., Fröhlich, F., Hasenauer, J., and Wren, J. (2018) PESTO: parameter estimation toolbox. *Bioinformatics* 34, 705–707.
17. St. John, P., Strutz, J., Broadbelt, L. J., Tyo, K. E. J., and Bomble, Y. J. (2018) Bayesian Inference of Metabolic Kinetics from Genome-Scale Multiomics Data. *bioRxiv*
18. Visser, D., and Heijnen, J. J. (2003) Dynamic simulation and metabolic re-design of a branched pathway using linlog kinetics. *Metabolic Engineering* 5, 164–176.
19. Liebermeister, W., and Noor, E. (2021) Model Balancing: A Search for In-Vivo Kinetic Constants and Consistent Metabolic States. *Metabolites* 11, 749.
20. Martinov, M. V., Vitvitsky, V. M., Mosharov, E. V., Banerjee, R., and Ataullakhanov, F. I. A Substrate Switch: A New Mode of Regulation in the Methionine Metabolic Pathway. *204*, 521–532.
21. Nijhout, H., Reed, M. C., Anderson, D. F., Mattingly, J. C., James, S. J., and Ulrich, C. M. Long-Range Allosteric Interactions between the Folate and Methionine Cycles Stabilize DNA Methylation Reaction Rate. *1*, 81–87.
22. Korendyaseva, T. K., Kuvatov, D. N., Volkov, V. A., Martinov, M. V., Vitvitsky, V. M., Banerjee, R., and Ataullakhanov, F. I. (2008) An Allosteric Mechanism for Switching between Parallel Tracks in Mammalian Sulfur Metabolism. *PLoS Computational Biology* 4, e1000076.
23. Poirier, D. J. (1998) REVISING BELIEFS IN NONIDENTIFIED MODELS. *Econometric Theory* 14, 483–509.
24. Van Rossum, G., and Drake, F. L. *Python 3 Reference Manual*; CreateSpace: Scotts Valley, CA, 2009.

25. Kacser, H., and Burns, J. A. (1973) The control of flux. *Symposia of the Society for Experimental Biology* 27, 65–104.
26. Noor, E., Flamholz, A., Liebermeister, W., Bar-Even, A., and Milo, R. (2013) A note on the kinetics of enzyme action: A decomposition that highlights thermodynamic effects. *FEBS Letters* 587, 2772–2777.
27. Liebermeister, W., Uhlenendorf, J., and Klipp, E. (2010) Modular rate laws for enzymatic reactions: thermodynamics, elasticities and implementation. *Bioinformatics* 26, 1528–1534.
28. Monod, J., Wyman, J., and Changeux, J. P. (1965) On the nature of allosteric transitions: a plausible model. *Journal of Molecular Biology* 12, 88–118.
29. Changeux, J.-P. (2013) 50 years of allosteric interactions: the twists and turns of the models. *Nature Reviews. Molecular Cell Biology* 14, 819–829, [text.sciwheel-projects](http://text.sciwheel-projects.org): Yeast.
30. Popova, S. V., and Sel'kov, E. E. (1975) Generalization of the model by Monod, Wyman and Changeux for the case of a reversible monosubstrate reaction SR,TP. *FEBS Letters* 53, 269–273.
31. Popova, S. V., and Sel'kov, E. E. (1979) [Description of the kinetics of the two substrate reactions S1+ S2 goes to and comes from S3+S4 by a generalized Monod, Wyman, Changeux model]. *Molekuliarnaiia Biologiia* 13, 129–139.
32. Matos, M. R. A., Saa, P. A., Cowie, N., Volkova, S., de Leeuw, M., and Nielsen, L. K. (2022) GRASP: A Computational Platform for Building Kinetic Models of Cellular Metabolism. *Bioinformatics Advances* 2, vbac066.
33. Dai, Z., and Locasale, J. W. (2017) Understanding Metabolism with Flux Analysis: From Theory to Application. *Metabolic Engineering* 43, 94–102.

34. Click Developers Click: Python Composable Command Line Interface Toolkit. Pallets, 2022; <https://pypi.org/project/click/>.
35. Pearson, W. Toml: Python Library for Tom’s Obvious, Minimal Language. 2020; <https://pypi.org/project/toml/>.
36. Pydantic developers Pydantic. 2022; <https://pypi.org/project/pydantic/>.
37. Carpenter, B., Gelman, A., Hoffman, M. D., Lee, D., Goodrich, B., Betancourt, M., Brubaker, M., Guo, J., Li, P., and Riddell, A. (2017) Stan: A Probabilistic Programming Language. *Journal of Statistical Software* 76, 1–32.
38. Stan Development Team CmdStanPy. 2022; <https://github.com/stan-dev/cmdstanpy>.
39. Betancourt, M. (2018) A Conceptual Introduction to Hamiltonian Monte Carlo. *arXiv:1701.02434 [stat]*
40. Kumar, R., Carroll, C., Hartikainen, A., and Martin, O. (2019) ArviZ a Unified Library for Exploratory Analysis of Bayesian Models in Python. *Journal of Open Source Software* 4, 1143.
41. Timonen, J., Siccha, N., Bales, B., Lähdesmäki, H., and Vehtari, A. An Importance Sampling Approach for Reliable and Efficient Inference in Bayesian Ordinary Differential Equation Models. 2022; <http://arxiv.org/abs/2205.09059>.
42. Serban, R., and Hindmarsh, A. C. CVODES: The Sensitivity-Enabled ODE Solver in SUNDIALS. Volume 6: 5th International Conference on Multibody Systems, Nonlinear Dynamics, and Control, Parts A, B, and C. Long Beach, California, USA, 2005; pp 257–269.
43. Margossian, C. Computing Steady States with Stan’s Nonlinear Algebraic Solver. Stan Conference 2018. 2018.